# Effects of morphological change on fluvial flood patterns evaluated by a hydro-geomorphological model

Jingming Hou, Hao Han, Zhanbin Li, Kaihua Guo and Yi Qin

## ABSTRACT

High aggradation and degradation in a river induced by the last flood event will raise and decrease the risk of an upcoming flood event, respectively. To quantitatively investigate this effect, a two-dimensional (2D) hydrodynamic model coupled with a sediment transport the river-bed evolution models is developed. After being validated against two experimental benchmark tests, the model is applied to simulate the effects of the morphological change on flood patterns. It is found in two experimental scale tests that bed evolution may have substantial influence on water level, which is directly related to flood risk extent. In the application of the model computing a realistic flood event in Bayangaole Reach of Yellow River, the results show that the water surface level becomes lower for an upcoming flood event with the same hydrograph, indicating the flood risk considerably decreases in the next flood event. The effect of a perturbed bed therefore could be of significance for fluvial flood over a movable bed and therefore to flood risk management.

**Key words** | flood, GPU, morphological change, sediment transport model, shallow water equations

**Jingming Hou** (corresponding author)
**Hao Han**
**Zhanbin Li**
**Kaihua Guo**
**Yi Qin**
School of Water Resources and Hydro-power Engineering,
Xi'an University of Technology,
No. 5 Jinhuan Road, Xi'an, Shaanxi 710048,
China
E-mail: *jingming.hou@xaut.edu.cn*

**Jingming Hou**
School of Civil Engineering and Geosciences,
Newcastle University,
Newcastle upon Tyne NE1 7RU,
UK

## INTRODUCTION

Morphological change is of importance for fluvial flood, especially for rivers with relatively high sediment concentration and a movable bed, e.g. the Yellow River in China. Different morphological characteristics of a river may affect the flood evolution process, for instance, an aggraded flood plain could raise the flood risk, causing immeasurable loss of life and property. On the other hand, a degraded river bed is likely to decrease the water surface level and reduce the flood risk. To reliably predict the flood risk, the morphological effects should be considered. Hydrodynamic models play a significant role in quantitatively evaluating the flood risk, for example, those in Song *et al.* (2011), Simons *et al.* (2014), and Liang & Smith (2015). The abovementioned models are able to simulate the flood propagation and inundation, however, the river bed evolution is not taken into account. Wu & Wang (2007) developed a one-dimensional (1D) model computing the flow, sediment transport and bed change. Compared with the 1D model, the two-dimensional (2D) model can calculate the flow variation, sediment transport rates, and river morphological changes during extreme flood events with greater accuracy, and achieve a good prediction of the amounts of material transport in the river (Gharbi *et al.* 2016). Some 2D hydro-geomorphological models have been proposed in recent years. Wu *et al.* (2012) presented a depth-averaged 2D model to compute the embankment break process which considers the flow and the bed change. Sun *et al.* (2015) proposed a robust 2D numerical model simulating a braided river based on non-uniform sediment transport assumption. Guan *et al.* (2015) developed a 2D coupled hydro-geomorphological model which could compute the complex solid–fluid interaction process. The model was combined with shallow water theory and a non-equilibrium assumption for sediment transport, aiming at simulating the morphological change caused by sediment-laden flows with various sediment transport modes.

doi: 10.2166/hydro.2018.142

The aforementioned model applications mainly look at the processes of flood causing sediment transport. It is obvious that river floods with high sediment transport capacity can result in erosion and deposition (Knight & Evans 2017) and the reshaped bed will in turn provide a new bathymetry for the flowing flood events, but the systematic research about river-bed evolution effects on flood propagation and inundation are very rare. Zhang *et al.* (2013) noticed that the free surface profiles were greatly influenced by bed change, through simulating dam-break flow over a movable bed. Pont *et al.* (2017) analysed the impact of two large floods on sediment deposition, observing a sea-level rising phenomenon due to the aggradation.

To quantitatively evaluate the morphological change effects on the flood propagation and inundation, this paper develops a hydrodynamic model coupled with morphological change to simulate such effects in the following section. The proposed model is then validated against two experimental benchmark tests considering both the suspended load and bed load. Then the model is adopted to evaluate the morphological effects on a realistic flood propagation and inundation, in order to show the flood pattern may be very different from that of a previous flood with a similar hydrograph, due to the perturbed topograph. Finally, brief conclusions are drawn.

## GOVERNING EQUATION AND NUMERICAL SCHEMES

The numerical model is governed by the shallow water equations coupled with the sediment transport and bed evolution equations:

$$\frac{\partial \boldsymbol{q}}{\partial t}+\frac{\partial \boldsymbol{f}}{\partial x}+\frac{\partial \boldsymbol{g}}{\partial y}=\boldsymbol{S},$$

$$\boldsymbol{q}=\begin{bmatrix}\eta\\ q_x\\ q_y\\ hC_s\\ hC_b\\ z_b\end{bmatrix},\ \boldsymbol{f}=\begin{bmatrix}q_x\\ uq_x+gh^2/2\\ uq_y\\ q_xC_s\\ \beta q_xC_b\\ 0\end{bmatrix},\ \boldsymbol{g}=\begin{bmatrix}q_y\\ vq_x\\ vq_y+gh^2/2\\ q_yC_s\\ \beta q_yC_b\\ 0\end{bmatrix},$$

$$\boldsymbol{S}=\begin{bmatrix}0\\ S_{bx}+S_{fx}\\ S_{by}+S_{fy}\\ E_s-D_s\\ E_b-D_b\\ \dfrac{D-E}{1-p}\end{bmatrix}=\begin{bmatrix}0\\ -\dfrac{gh\partial z_b}{\partial x}-C_fu\sqrt{u^2+v^2}\\ -\dfrac{gh\partial z_b}{\partial y}-C_fv\sqrt{u^2+v^2}\\ \varpi_0(C_{sae}-C_{sa})\\ -\dfrac{(q_xC_b-\beta q^*)}{L}\\ \dfrac{1}{1-p}\left[\alpha\left(\dfrac{q_xC_b-q^*}{\beta L}\right)+\varpi_0(1-\alpha)(C_{sa}-C_{sae})\right]\end{bmatrix}.$$

where $\boldsymbol{q}$ is the variable vector consisting of the water level $\eta$, $q_x$ and $q_y$ (unit-width discharges in the x and y direction), $hC_s$ and $hC_b$ (conservative concentration of suspended load and bed load, respectively) and bed elevation $z_b$ (Guan *et al.* 2014); $h$ denotes the water depth following the relationship of $\eta=z_b+h$ (Guan *et al.* 2014); $\boldsymbol{f}$ and $\boldsymbol{g}$ are the flux vectors in the x and y directions, respectively; $u$ and $v$ are the velocity components in the two Cartesian directions and $q_x=uh$, $q_y=vh$; $g$ represents the gravity acceleration with a value of 9.81 m s$^{-2}$ (Guan *et al.* 2014, 2015); $\boldsymbol{S}$ is the source vector; $S_b$ and $S_f$ are the source terms of bed slope and friction, respectively (Guan *et al.* 2014; 2015); $D$ and $E$ denote the deposition and entrainment rates, respectively, and the subscripts $s$ and $b$ are suspended load and bed load, respectively (Guan *et al.* 2015); $C_f$ is the bed roughness coefficient controlled by the Manning coefficient $n$ and water depth in the form of $C_f=gn^2/h^{1/3}$. Regarding the sediment parameters, $\varpi_0$ is the settling velocity of single sediment particles (van Rijn 1984); $C_{sa}=C_s\delta$ means the near-bed concentration at a reference level, $\delta$ is computed as that in Cao *et al.* (2004); $C_{sae}$ represents the near-bed equilibrium concentration at a reference level, computed by the function presented in Smith & Mclean (1997) as $C_{sae}=0.00156T/(1+0.0024T)$, and $T=(\theta-\theta_{cr})/\theta_{cr}$, where $\theta$ and $\theta_{cr}$ are Shields parameter and critical Shields parameter, respectively; $\beta$ denotes the difference of the velocities of the sediment phase and the fluid water (Greimann *et al.* 2008), $\beta=1$ is assumed by

Guan *et al.* (2014); $q^*$ is the unit-width sediment transport capacity evaluated by the Meyer Peter and Müller equation (Guan *et al.* 2015); $L$ is the non-equilibrium adaptation length of sediment transport (Guan *et al.* 2014), computed by $L = h\sqrt{u^2+v^2}/\gamma\omega$, and $\gamma = \min(\beta h/h_b,\ (1-p)/C_b)$, where $h_b = \mu\theta d_{50}$, $d_{50}$ = the 50th percentile grain size, $\mu$ is suggested from 6 to 12 (Guan *et al.* 2014). As tested, the results are not sensitive to $\mu$ higher than 8, meanwhile, $\mu = 9$ can produce relatively reliable modelling results, so $\mu = 9$ is adopted in this work; $p$ is the porosity of the bed material (Guan *et al.* 2014); $\alpha$ is the weight coefficient of sediment types (Guan *et al.* 2015). Most of the sediment parameters are determined via empirical formula.

The governing equations above are numerically solved by a Godunov-type finite volume scheme as presented in other papers of the authors, e.g. Hou *et al.* (2013a, 2013b). The numerical scheme is able to well preserve the mass conservation property. In this model, the Harten, Lax and van Leer approximate Riemann solver with the contact wave restored (HLLC) is applied to compute the numerical fluxes of water, momentum and sediment across cell interfaces. The HLLC approximate Riemann solver could capture the shock wave in a very robust way. The required face values of the flow and sediment variables are evaluated by using a MUSCL scheme to achieve second order accuracy and avoid the numerical oscillations. They are also reconstructed by using a non-negative depth reconstruction method to preserve the well balanced condition or conservation property (C-property) (Hou *et al.* 2013a). The slope source terms are evaluated by the slope-flux method proposed in Hou *et al.* (2013a). The friction source terms are computed using a splitting point-implicit method as in Liang & Marche (2009). The time marching is achieved by using a two-stage explicit Runge-Kutta time-integration scheme. The Courant-Friedrichs-Lewy (CFL) condition is used to control the time steps so as to maintain the robustness. To handle the problem of the numerical instabilities caused by the wetting and drying over complex topography, the approach presented in Hou *et al.* (2013b) is adopted. It should be mentioned that the hydrodynamic and sediment transport governing equations are solved in a fully coupled way. The numerical model is programmed by applying the CUDA code which could considerably accelerate the computation on GPUs (Graphic Processing Units) (Liang & Smith 2015), aiming to release the computational burden for practical large-scale applications with relatively high resolution. In this work, a desktop with a *NVIDIA GeForce GTX* 980Ti GPU is used to run all simulations.

## SIMULATION OF DAM-BREAK FLOOD OVER A MOVABLE BED

An experimental test investigated in the laboratory of UCL in Belgium (Goutiere *et al.* 2011) is reproduced to verify the capability of the current model in simulating the hydro-geomorphological processes induced by a dam break. As shown in Figure 1 (Goutiere *et al.* 2011), the initial still water depths before and after the gate located at $x = 3.5$ m are 0.25 and 0 m, respectively, within a domain of 6 and 0.5 m in x and

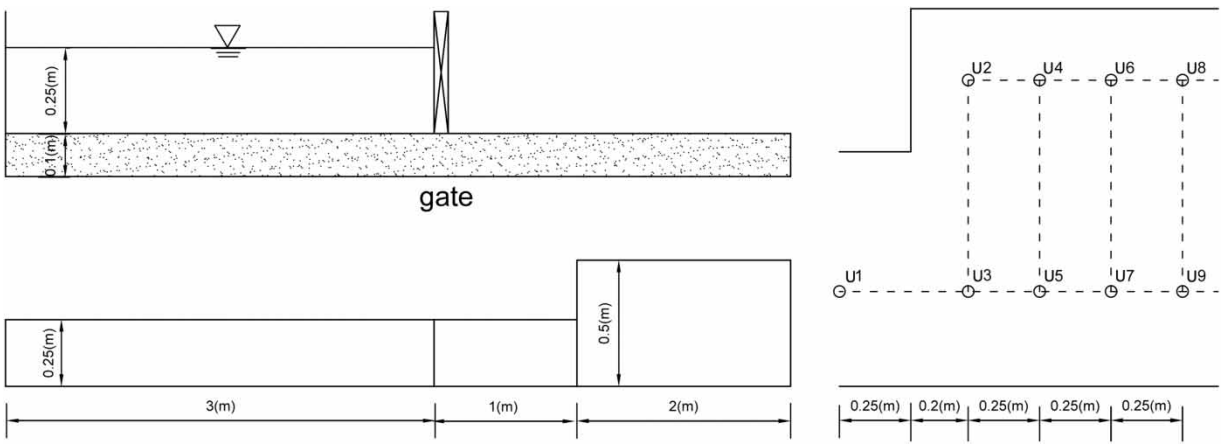


**Figure 1** | Sketch of a dam-break flow experiment over a mobile bed.

y directions. A 0.1 m thick movable bed consists of saturated bed sand with a median diameter of 1.72 mm. The sediment porosity is 0.39 (Guan *et al.* 2014). The Manning coefficient is assumed to be 0.023 s $m^{-1/3}$ as suggested in Guan *et al.* (2015) and Goutiere *et al.* (2011). The computational domain is discretized into 120,000 squared cells with the size of 0.005 m. Courant number is 0.4 for all the simulations.

As plotted in Figure 2, the computed water levels at Gauges U2 [4.20, 0.375] and U6 [4.70, 0.375] are compared with the measured ones. A good agreement indicates the model can reliably predict the flows over the erodible bed. Besides, the morphological change is simulated as well as shown in Figure 3. Figure 4 shows the new morphological change for the following flood event. This figure reveals that the bed erosion occurs near the sudden expansion based on the simulation results of the computed bed change and the original, and shows the modelled bed elevation at $t = 1$ and 10 s. A pit and a sand bar can be clearly observed between the part of $y =$ 4 and 5 m, consistent with that in Guan *et al.* (2015) and Goutiere *et al.* (2011). The computed bed after flush is also compared with the available measured ones at the cross sections of $y =$ 4.3 and 4.5 m. As plotted in Figure 5, the trend of bed change is correctly evaluated by the current model, confirming the model is able to predict hydro-geomorphological problems caused by flow over erodible bed. The computational time for this test case on GPU and CPU is 312.7 and 4,883.6 s, respectively, i.e. the GPU can accelerate the computation by 15.6 times.

To reflect the bed change effect on flood inundation, the new bed after 15 s is used as initial bed for simulating the next flood event caused by the same dam-break condition. The water level and the bed at two cross sections of $y = 4.3$ and 4.5 m are shown in Figure 6. It is clear that the water level for the following flood event may be considerably different from that of the previous flood, on average 0.02 m lower than the previous water level on the left side and on average 0.04 m higher than the previous water level on the right side (Figure 6(a)), indicating that the morphological change has a remarkable effect on the flood propagation and inundation process. Accurate flood risk analysis should take account of the morphological factor for a river relevant to a movable river bed.

## SIMULATION OF FLOW AND SEDIMENT TRANSPORT OVER A TRENCH

The experiments conducted at the Delft Hydraulics Laboratory (Guan *et al.* 2015) were reproduced to verify the capability of the model to simulate the bed evolution process caused by the suspended load and bed load. The bed change effect on flood pattern is also investigated. In the experiment, the water and sediment move over a channel with a trench whose side slopes are 1:10 (Figure 7). The water

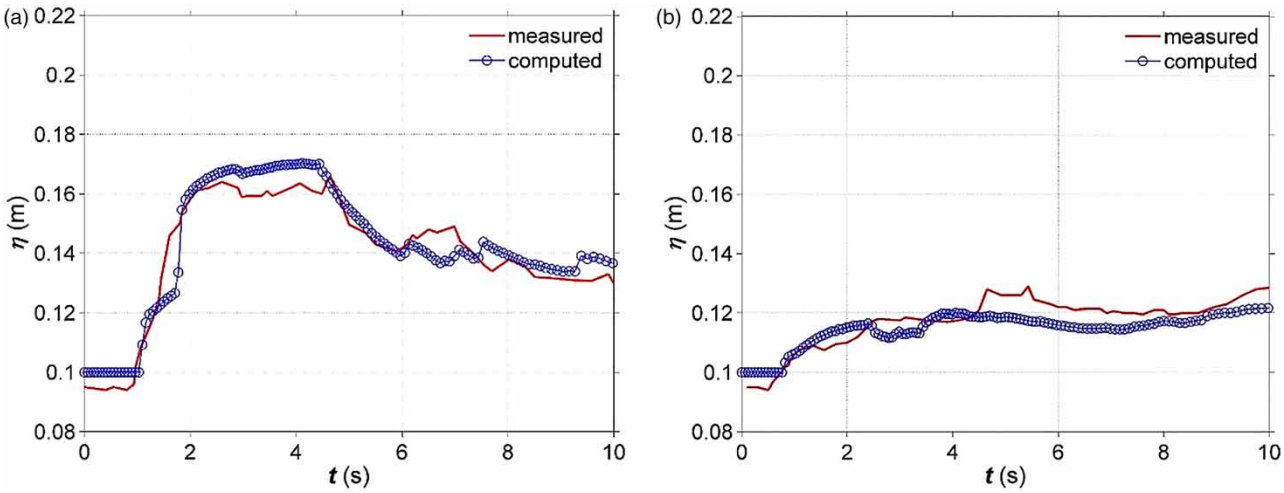


**Figure 2** | Computed and measured water levels at (a) Gauge U2; (b) Gauge U6.

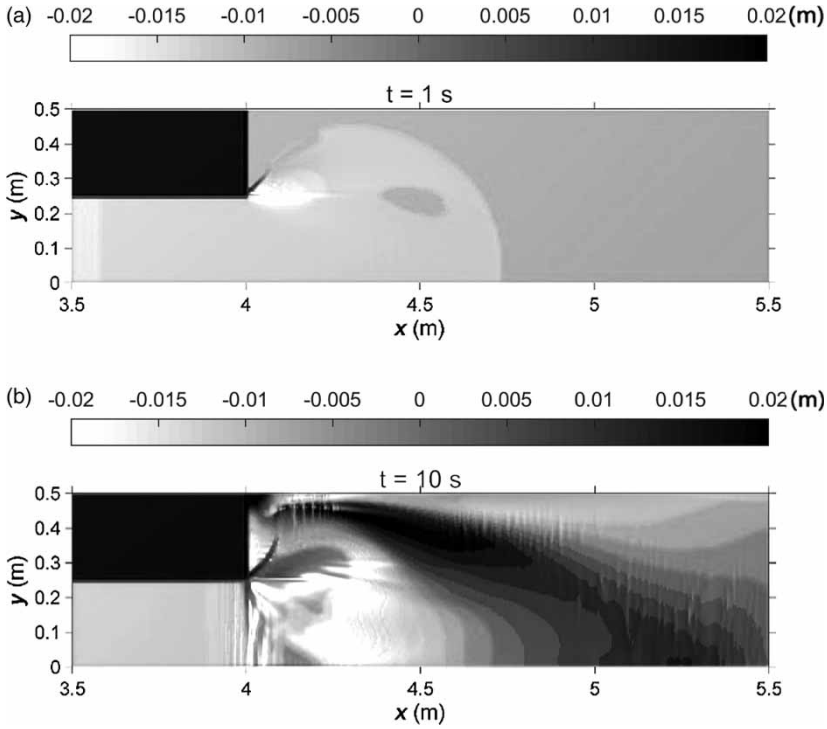


**Figure 3** | Computed bed change compared to the original bed at (a) $t = 1$ s; (b) $t = 10$ s.

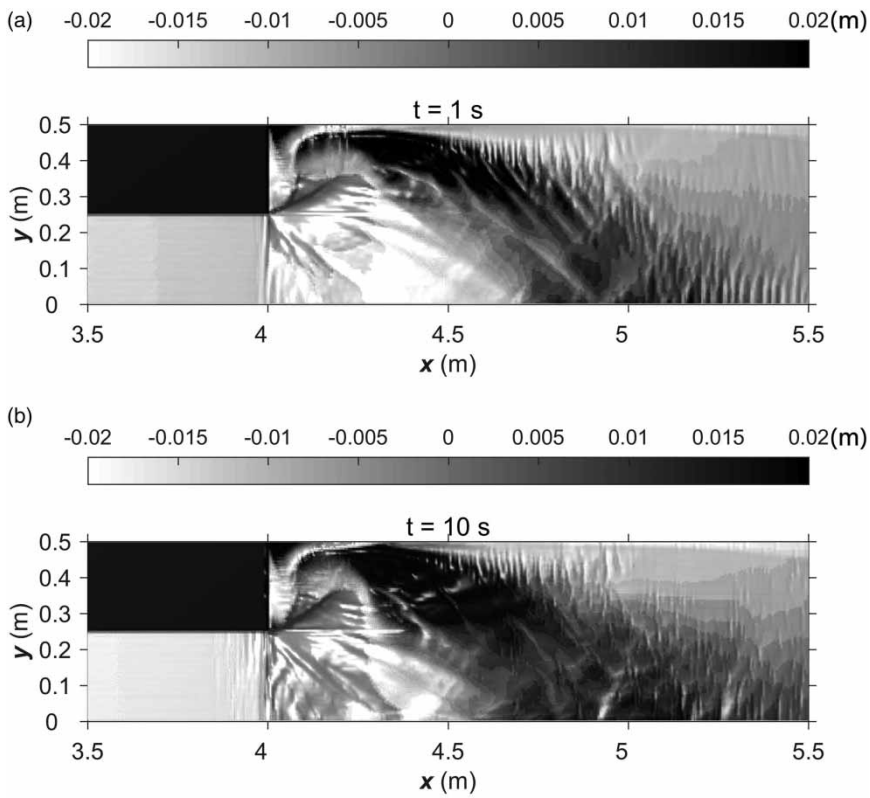


**Figure 4** | Computed new bed change compared to the original bed at (a) $t = 1$ s; (b) $t = 10$ s.

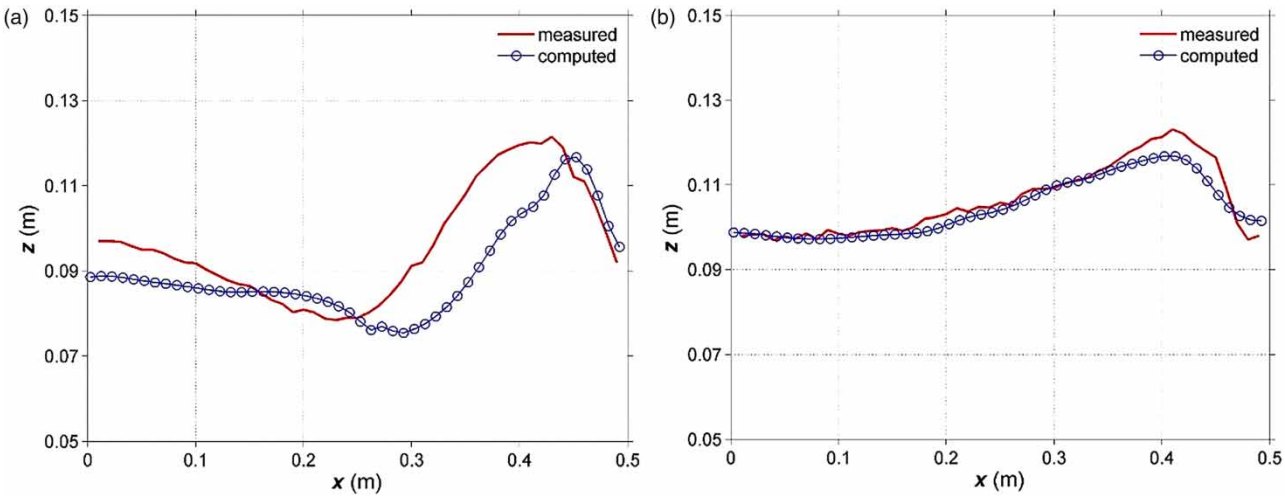


**Figure 5** | Computed and measured beds at the cross sections of (a) $y = 4.3$ m; (b) $y = 4.5$ m.

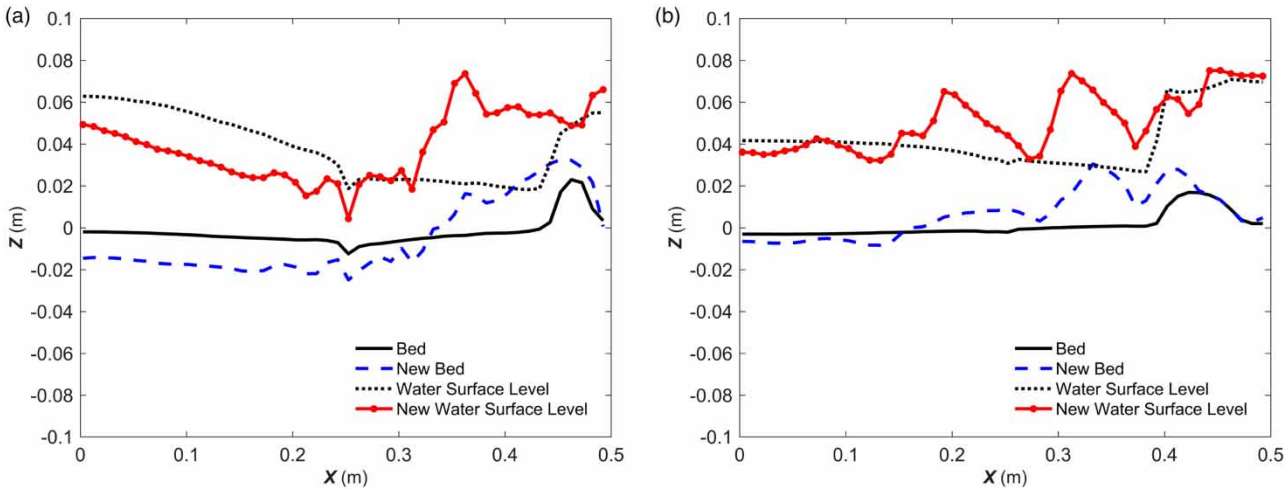


**Figure 6** | Comparison between the water level and the river bed of $y = 4.3$ m (a) and $y = 4.5$ m (b) at $t = 2$ s for the two sediment events ('New' means the following flood event).

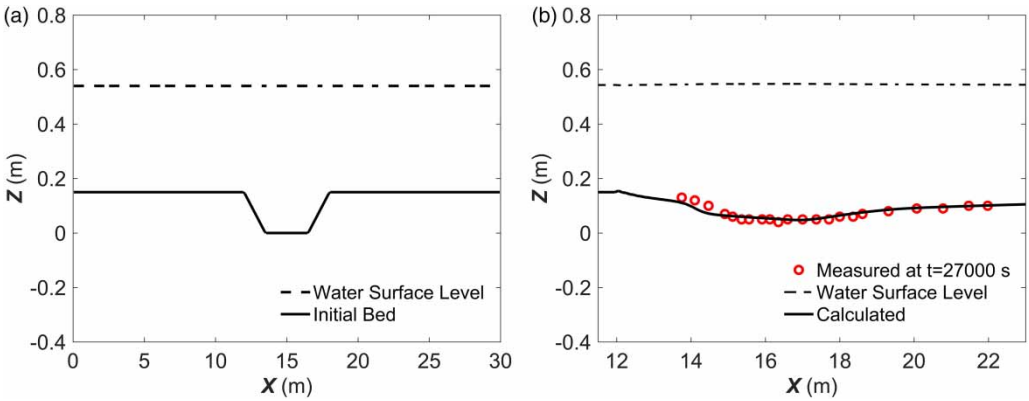


**Figure 7** | The initial bed elevation at the vertical section (a) and the simulation result (b) at t = 27,000 s.

depth is 0.39 m, and the initial flow velocity is 0.51 m $s^{-1}$ in the x direction. The channel bed is covered by fine sand with a median diameter of 0.16 mm. The sand density and porosity are 2,650 kg $m^{-3}$ and 0.4, respectively. The Manning coefficient is set to be 0.016 s $m^{-1/3}$. The computational domain is discretized into 3,000 squared cells with the size of 0.1 m. Herein, $\alpha$ is the weighting coefficient for bed load and suspended load transport and $\alpha = 0.25$ was suggested as in Guan *et al.* (2015).

The model was run for 4,800 s to achieve a steady flow. Figure 7(b) shows the computed result at time of 27,000 s. The trench shape changes becomes smoother as a result of the scour and sedimentation. Comparing with the experimental results in terms of the bed elevation, the modelled bed is in fairly good agreement with the measured data, illustrating that the proposed model is able to reproduce the sediment transport and the morphological change process caused by both suspended load and bed load. Furthermore, the flow with a constant unit-width discharge of 0.1989 $m^2$ $s^{-1}$ is well computed, showing that the flow pattern can be reliably modelled as well. The running time for simulating the 7.5 h event is 507 s on a GPU, the computational efficiency is therefore relatively high.

To evaluate the bed evolution effects on flood propagation and inundation process, a following flood event is modelled, using changed bed at t = 7.5 h as the initial condition with the same flow property. The computed bed evolution process is plotted in Figure 8 which shows a different bed profile. For the flow over the new bed, the computed water level is slightly higher than that of the previous flood event, about 1% higher is shown in Figure 9(a), indicating the bed change in last flood event will slightly increase the

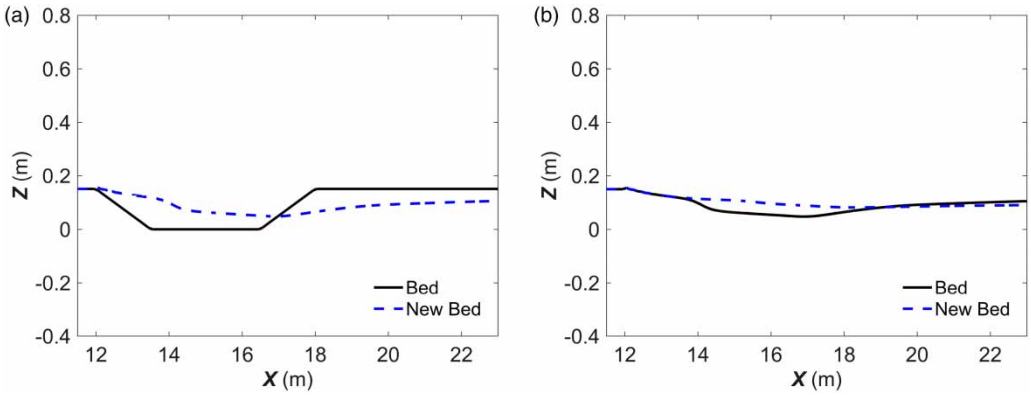


**Figure 8** | Comparison between the bed at $t = 0$ h (a) and at $t = 7.5$ h (b) for the two sediment transport events ('New' means the following flow event).

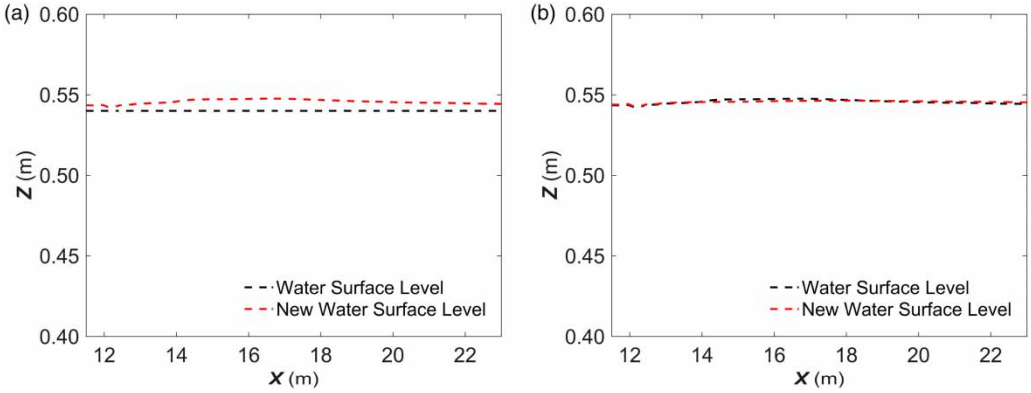


**Figure 9** | Comparison between the water level and the new water level bed at $t = 0$ h (a) and at $t = 7.5$ h (b).

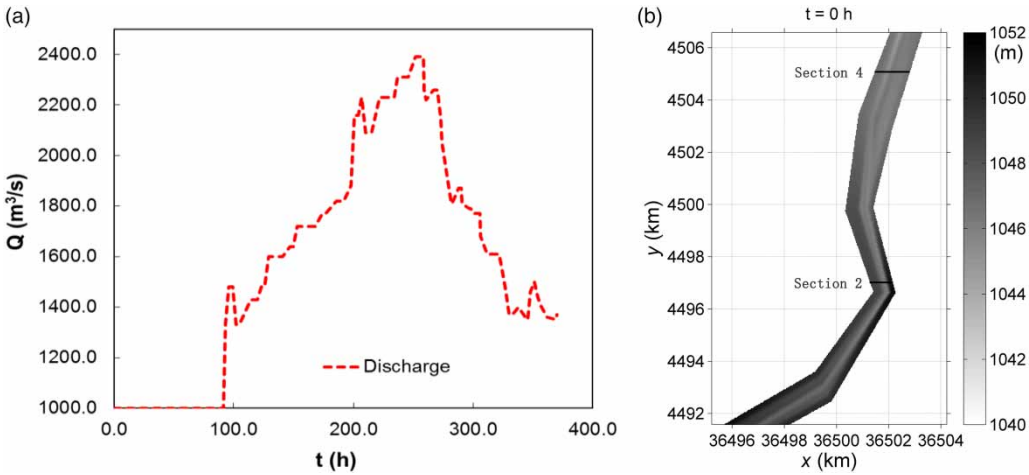


**Figure 10** | Inflow hydrograph (a) and the initial bed elevation (b) at the Bayangaole Reach of Yellow River.

flood risk in the next event. However, the change is not so obvious perhaps as a result of the subcritical flow condition.

## APPLICATION TO BAYANGAOLE REACH OF YELLOW RIVER

In this section, the proposed model is used to investigate the morphological dynamics in the Bayangaole reach of Yellow River, China, during a real flood event in 2002 and a fictitious one with the same hydrograph. The inflow hydrograph and the initial bed elevation are sketched in Figure 10. The flood enters the domain from south to north, i.e. the inflow boundary is located at the lower part of the domain (Figure 10(b)). The reach is about 15 km long and 1 km wide and consists of 66,511 squared cells with the size of 30 m. The river banks are assumed as closed boundaries and the north boundary is set as open. The median diameters of the suspended load and bed load are considered as 0.05 and 0.18 mm, respectively. 0.015 and 0.0017 are imposed at the inflow boundary for the volumetric concentration of the suspended load and bed load, respectively, equivalent to about 40 and 4.5 kg m$^{-3}$ in weight concentration. A constant Manning coefficient is adopted as 0.02 s m$^{-1/3}$. The initial condition is achieved by running the model under the condition of a constant

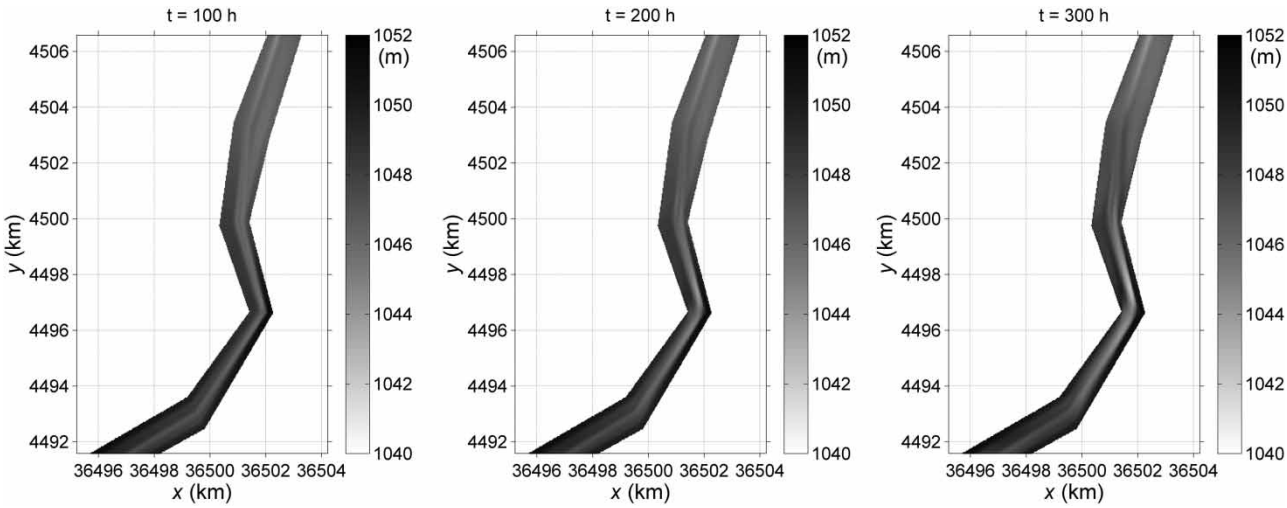


**Figure 11** | Computed bed evolution at the Bayangaole Reach of Yellow River.

inflow discharge of 1,000 $m^3 s^{-1}$ and fixed bed until reaching a steady stage. Then the model is run for 300 h with the hydrograph plotted in Figure 10(a) and a constant discharge of 1,000 $m^3 s^{-1}$ for 500 h longer to simulate the river recovery process.

Figure 11 plots the morphological change over 300 h and scour is observed in the middle reach. This feature is also sketched in Figure 12 which shows the computed bed change compared to the original one. The positive values means deposition and negative ones denotes the erosion. It is clearly observed that the deposition and erosion occur in the lower reach (north part) and middle reach, respectively. Li *et al.* (2016) analyzed the coarse sediment movement in the flood event under consideration in Inner Mongolia Reach of Yellow River, and found the bed erosion appeared in the downstream of the studied area, proving the reliability of the proposed model. Figure 13 depicts the evolution of the computed water depth, indicating the water depth becomes greater and greater in the middle reach due to scour. It also shows the river starts to be more and more braided in the lower reach.

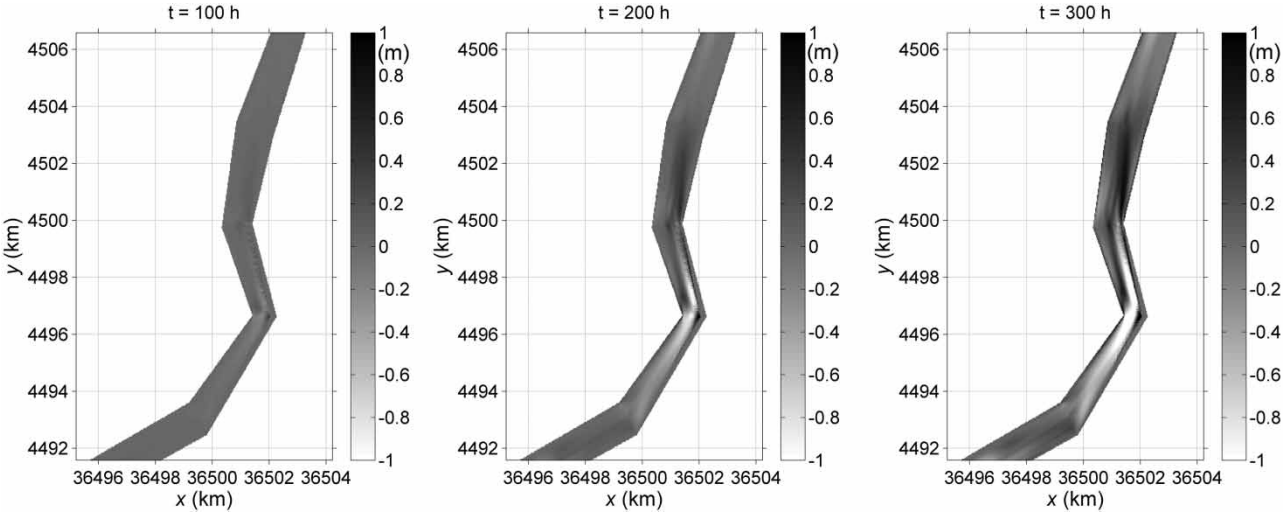


**Figure 12** | Computed bed change compared with that at the Bayangaole Reach of Yellow River.

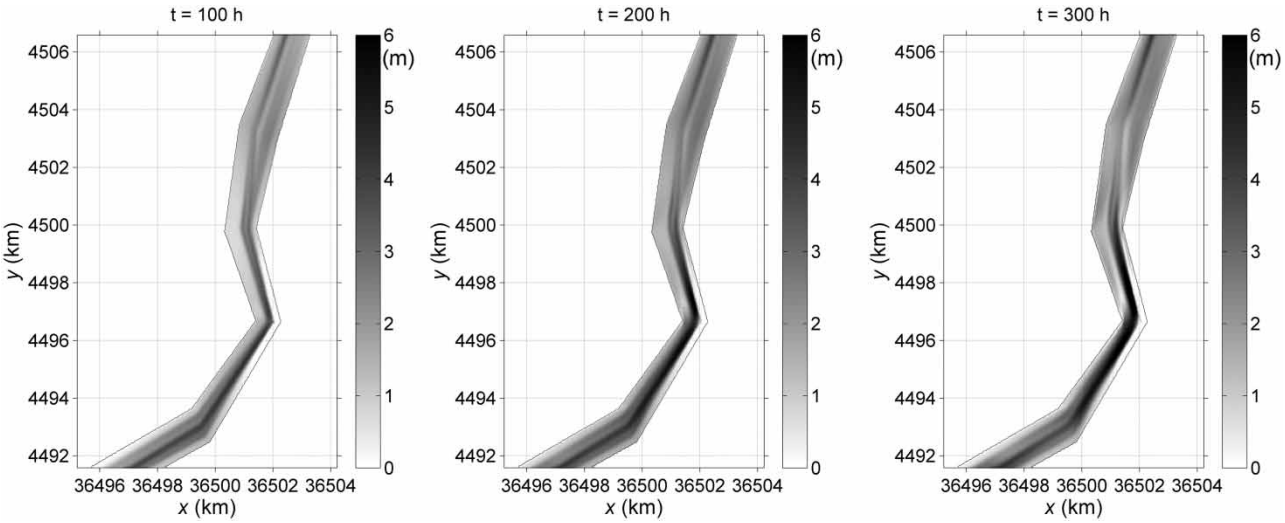


**Figure 13** | Computed water depth evolution over the movable bed at the Bayangaole Reach of Yellow River.

After 800 h, the new bed is used as initial bed for an upcoming flood event, in order to quantitatively evaluate the effects of the morphological change. The new initial bed is almost the same as that in the left subfigure in Figure 14. The following flood lasts for 300 h with the same inflow hydrograph plotted in Figure 10(a). Figures 14 and 15 sketch the morphological change process. An overall erosion pattern is observed except for the part close to the outlet. It is slightly different with the previous event. Figure 16 shows the computed water depth at $t = 100$, 200 and 300 h, indicating that the river becomes deeper in the middle reach and more braided in the lower reach. This feature is also plotted in Figure 17 at two cross sections of $y =$ 4, 497 and 4,505 km. The computed water levels and bed for the two flood events are compared in Figure 17, illustrating that the water surface level becomes lower in the following flood event due to bed erosion. It also indicates that the flood risk markedly decreases for the following flood event in this reach, i.e. a flood with a similar hydrograph may cause very different

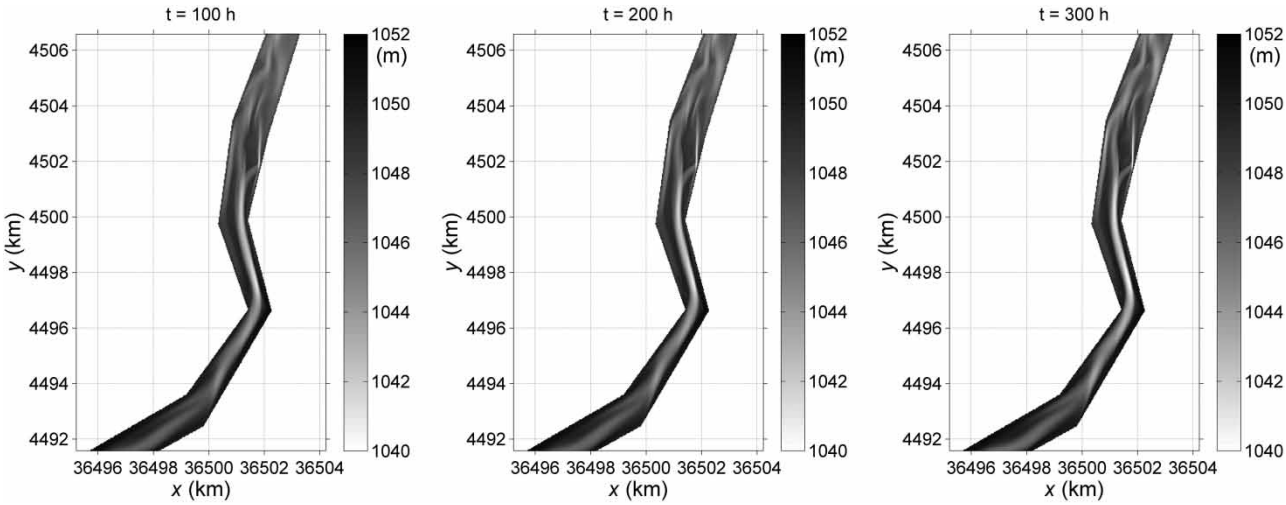


**Figure 14** | Computed bed evolution at the Bayangaole Reach of Yellow River for a following flood event.

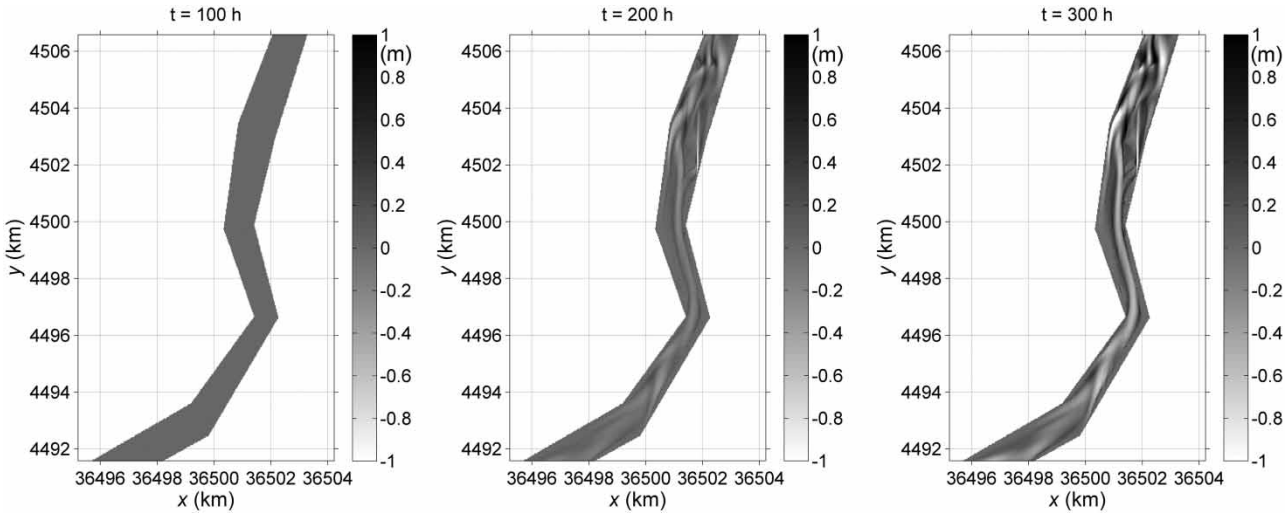


**Figure 15** | Computed bed change compared with the original at the Bayangaole Reach of Yellow River for a following flood event.

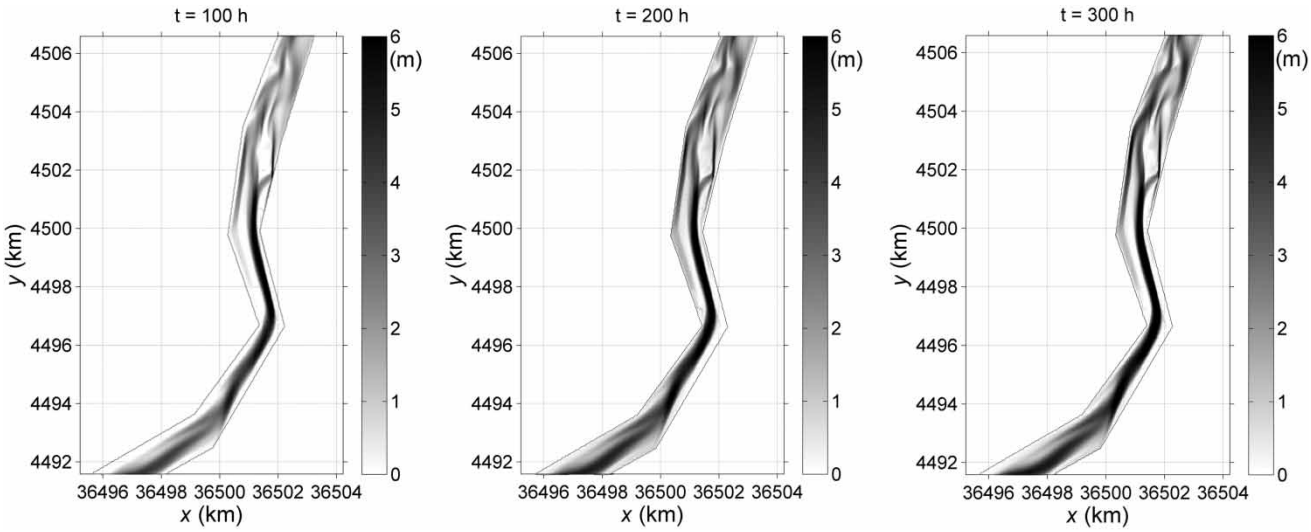


**Figure 16** | Computed water depth evolution over the movable bed at the Bayangaole Reach of Yellow River for a following flood event.

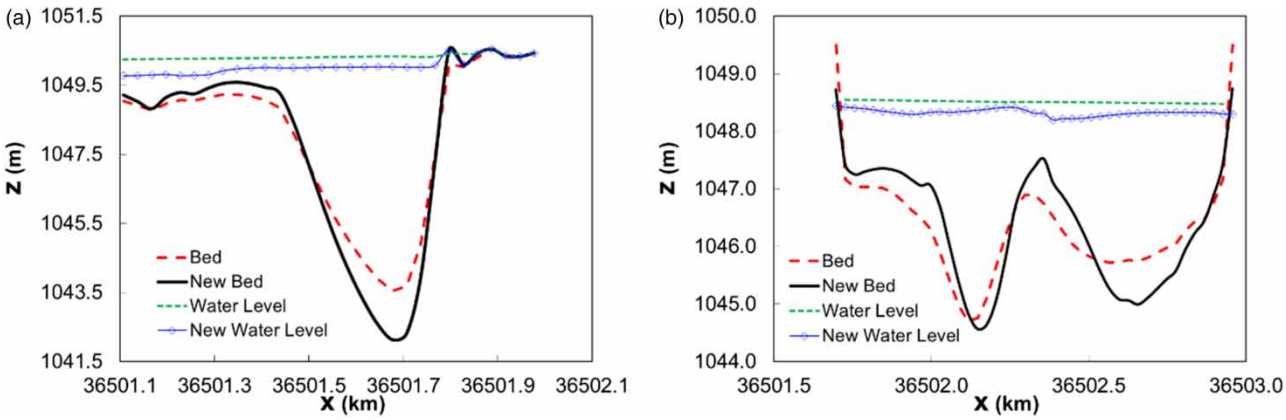


**Figure 17** | Comparison between the water level and the river bed at Section 2 (a) and 4 (b) at t = 200 h for the two flood events ('New' means the following flood event).

propagation and inundation patterns due to morphological change.

## CONCLUSIONS

In this work, a GPU based hydro-geomorphological model is developed and validated against two experimental benchmark tests. Through comparison with the measured flow and bed data, the computed results are seen to be in a fairly good agreement, thus showing the model could produce reliable results for modelling the flow patterns, sediment transport for both suspended load and bed load, as well as the bed evolution process. The GPU code could accelerate the computation in an effective way. The model is adopted to quantitatively evaluate bed evolution caused by an additional flood and the effects of the morphological change on the flood propagation and inundation, illustrating that the bed evolution may have substantial influence on water levels which are related to flood risk extent in two experimental scale tests. The model is also adopted to model a realistic flood event in Bayangaole Reach of Yellow River. It found that the flood lead to scour and braided form in the middle and lower reach, respectively.

As a result, the water surface level becomes lower for an upcoming flood event with the same hydrograph, indicating the flood risk considerably decreases in this event. This means, for a fluvial flood with movable bed, the morphological effect is by no means trivial to reliably predict the flood risk and should be properly taken into account during the planning, design, construction and management relating to flood risk evaluation.

## ACKNOWLEDGEMENTS

This work is partly supported by the National Key Research Program of China (2016YFC0402704); National Natural Science Foundation of China (19672016); State Key Program of National Natural Science Foundation of China (Grant No. 41330858) and the UK Natural Environment Research Council (NERC) (Grant No. NE/K008781/1).

## REFERENCES

Cao, Z., Pender, G., Wallis, S. & Carling, P. 2004 Computational dam-break hydraulics over erodible sediment bed. *Journal of Hydraulic Engineering* **130**, 689–703.

Gharbi, M., Soualmia, A., Dartus, D. & Masbernat, L. 2016 Floods effects on rivers morphological changes application to the Medjerda river in Tunisia. *Journal of Hydrology & Hydromechanics* **64**, 56–66.

Goutiere, L., Soares-Frazão, S. & Zech, Y. 2011 Dam-break flow on mobile bed in abruptly widening channel: experimental data. *Journal of Hydraulic Research* **49**, 367–371.

Greimann, B., Yong, L. & Huang, J. C. 2008 Two-dimensional total sediment load model equations. *Journal of Hydraulic Engineering* **134**, 1142–1146.

Guan, M., Wright, N. G. & Sleigh, A. 2014 2D process based morphodynamic model for flooding by non-cohesive dyke breach. *Journal of Hydraulic Engineering* **140**, 44–51.

Guan, M., Wright, N. G. & Sleigh, A. 2015 Multimode morphodynamic model for sediment-laden flows and geomorphic impacts. *Journal of Hydraulic Engineering* **141**. doi:10.1061/(ASCE)HY.1943-7900.0000997.

Hou, J., Liang, Q., Simons, F. & Hinkelmann, R. 2013a A 2D well balanced shallow flow model for unstructured grids with novel slope source term treatment. *Advances in Water Resources* **52**, 107–131.

Hou, J., Liang, Q., Simons, F. & Hinkelmann, R. 2013b A stable 2D unstructured shallow flow model for simulations of wetting and drying over rough terrains. *Computers & Fluids* **82**, 132–147.

Knight, J. & Evans, M. 2017 The sediment stratigraphy of a flood event: an example from the Sabie River, South Africa. *Catena* **151**, 87–97.

Li, Z., Qin, Y., Chen, X., Wang, W. & Wu, Q. 2016 Effects of the coarse sediment movement in the flood on Inner Mongolia Reach of Yellow River in 2012. *Advances in Water Science* **27**, 687–695.

Liang, Q. & Marche, F. 2009 Numerical resolution of well-balanced shallow water equations with complex source terms. *Advances in Water Resources* **32**, 873–884.

Liang, Q. & Smith, L. S. 2015 A high-performance integrated hydrodynamic modelling system for urban flood simulations. *Journal of Hydroinformatics* **17**, 518–533.

Pont, D., Day, J. W. & Ibáñez, C. 2017 The impact of two large floods (1993–1994) on sediment deposition in the Rhône Delta: implications for sustainable management. *Science of the Total Environment* **609**, 251–262.

Simons, F., Busse, T., Hou, J., Özgen, I. & Hinkelmann, R. 2014 A model for overland flow and associated processes within the hydroinformatics modelling system. *Journal of Hydroinformatics* **16**, 375–391.

Smith, J. D. & Mclean, S. R. 1977 Spatially averaged flow over a wavy surface. *Journal of Geophysical Research* **82**, 1735–1746.

Song, L., Zhou, J., Guo, J., Zou, Q. & Liu, Y. 2011 A robust well-balanced finite volume model for shallow water flows with wetting and drying over irregular terrain. *Advances in Water Resources* **34**, 915–932.

Sun, J., Lin, B. & Yang, H. 2015 Development and application of a braided river model with non-uniform sediment transport. *Advances in Water Resources* **81**, 62–74.

Van Rijn, L. C. 1984 Sediment transport, part II: suspended load transport. *Journal of Hydraulic Engineering* **110**, 1613–1641.

Wu, W. & Wang, S. S. Y. 2007 One-dimensional modeling of dam-break flow over movable beds. *Journal of Hydraulic Engineering* **133**, 48–58.

Wu, W., Marsooli, R. & He, Z. 2012 Depth-averaged two-dimensional model of unsteady flow and sediment transport due to noncohesive embankment break/breaching. *Journal of Hydraulic Engineering* **138**, 503–516.

Zhang, S., Duan, J. G. & Strelkoff, T. S. 2013 Grain-scale nonequilibrium sediment-transport model for unsteady flow. *Journal of Hydraulic Engineering* **139**, 22–36.

First received 27 October 2017; accepted in revised form 27 December 2017. Available online 13 February 2018